ELSEVIER

Journal of Non-Crystalline Solids 272 (2000) 200–208

JOURNAL OF NON-CRYSTALLINE SOLIDS

www.elsevier.com/locate/jnoncrysol

High photoluminescence in erbium-doped chalcogenide thin films

J. Fick [a,*], É.J. Knystautas [a], A. Villeneuve [a], F. Schiettekatte [b], S. Roorda [b], K.A. Richardson [c]

[a] *Centre d'Optique, Photonique et Laser, Université Laval, Cité Universitaire, Que. G1K 7P4, Canada*
[b] *Département de physique, Université de Montréal, Montréal, Que. H3T 1J4, Canada*
[c] *CREOL, University of Central Florida, 4000 Central Florida Blvd., Orlando, FL 32816, USA*

Received 6 December 1999

Abstract

The spectral properties of the chalcogenide glasses As_2S_3 and $As_{24}S_{38}Se_{38}$-doped with Er^{3+} are presented and discussed. Thin films were formed by thermal evaporation and the erbium doping was obtained by subsequent ion implantation. Strong Er^{3+} emission at 1.54 μm has been observed. The high refractive index of these chalcogenide glasses lead to Er^{3+} emission cross-sections (15×10^{-21} cm^2) which are two times higher than for doped silica glass. The lifetime of the Er^{3+} metastable $^4I_{13/2}$ energy level was measured to be 2.3 ms. This short lifetime is consistent with the high emission cross-section. Furthermore, the very low phonon energies of chalcogenide glasses lead to relatively long lifetimes of the Er^{3+} $^4I_{11/2}$ pump level, which have been measured to be of the order of 0.25 ms. These spectral properties make this glass a good candidate for applications in the field of integrated optics.

PACS: 81.15.Kk; 78.55.Hx; 42.79.Gn; 61.43.Dq

1. Introduction

The erbium-doped fibre amplifier (EDFA) has produced revolutionary changes in communication technologies and most of the actual telecommunication systems depend on this device. But the integration of different optical functions on small devices requires a more compact optical amplifier. The development of short optical amplifiers suffers from concentration quenching effects caused by the high erbium concentration, which is needed to compensate for the short interaction length. The choice of a well-adapted host material and its careful development becomes therefore very critical for the successful realisation of integrated optical amplifiers.

The unique optical properties found in chalcogenide glasses make them very interesting for integrated optical devices. These include low phonon energies and high linear refractive index, which make chalcogenide glasses a very good host for rare earth doping. The lack of the hydroxyl absorption at 1.44 μm allows, in principle, the realisation of a broadband amplifier working between 1.2 and 1.7 μm. But these glasses have also

* Corresponding author. Permanent Address: LEMO-ENSERG, 23 Avenue des Martyrs, B.P. 257, F-38016 Grenoble cedex, France. Tel.: +33-4 76 85 60 19; fax: +33-4 76 85 60 80.
E-mail address: fick@enserg.fr (J. Fick).

0022-3093/00/$ - see front matter
PII: S0022-3093(00)00119-8

other advantages. Their high photosensitivity can be used for Bragg-grating fabrication [1]. Moreover, chalcogenide glasses show a very high optical non-linearity. The non-linear refractive index n_2 of $As_{24}S_{38}Se_{38}$ was measured to be almost two orders of magnitude higher than that of silica [2]. By exploiting all these properties, it is possible to realise advanced integrated optical devices such as mode-locked lasers in a single material. Bulk chalcogenide glass of high optical quality is easily fabricated and thin films can be obtained by sputtering [3], laser ablation [4], chemical vapour deposition [5] or thermal evaporation [6–8]. The film patterning can be done by laser beam writing, ion implantation or standard wet etching techniques [9].

Work on rare-earth-doped chalcogenide glass has been published for bulk materials [10–12] and thin films [3,6]. The respective evaporation rates of chalcogenide glass and rare-earth atoms are so different that thermal evaporation leads to nearly undoped films. For this reason we decided to use ion implantation, which is a widely used technique for rare earth doping of thin film photonic materials [13].

The present work was preceded by the study of the spectral properties of neodymium-doped As_2S_3 films [6]. Encouraged by the good results of this work, we enlarged our research on erbium-doped chalcogenide glass. In this paper, we report on the spectral properties of erbium-implanted As_2S_3 and $As_{24}S_{38}Se_{38}$ thin films. The composition $As_{24}S_{38}Se_{38}$ was chosen because it shows the highest optical non-linearity of the As:S:Se glass system [2]. The fabrication and implantation procedures are discussed and the results of photoluminescence, excitation and lifetime measurements are reported and compared for different samples.

2. Experimental

2.1. Thin film fabrication

Two kinds of thin film structures were studied: As_2S_3 single-layers and $As_2S_3/As_{24}S_{38}Se_{38}/As_2S_3$ multi-layer samples. The films were thermally evaporated onto slowly rotating oxidised silicon (SiO_2/Si) wafers. The evaporation rate was 1–2 nm/s and the pressure was 2×10^{-7} Torr. After the evaporation process the film thickness was checked using a Sloan Dektak II profilometer. Commercially available As_2S_3 glass from Amorphous Materials was used as source material for the arsenic-tri-sulphide films. In the case of $As_{24}S_{38}Se_{38}$ we used ground bulk glass prepared using standard techniques from elemental starting materials in sealed quartz ampoules [2]. The pure As_2S_3 single-layers received a post-deposition heat treatment at 165°C for 2 h with subsequent cooling at a rate of 1°C/min. Two samples underwent a second identical annealing process after ion implantation.

The possibility of installing two evaporation boats into our vacuum chamber allows multi-layer deposition without opening the chamber. However, because of the shallow penetration depth of the erbium ions, the erbium implantation was performed before the evaporation of the last As_2S_3 layer. After the deposition of this last layer, the samples were annealed at 135°C for 2 h with subsequent cooling at a rate of 1°C/min.

To fabricate channel waveguides on the single-layers, 1.2 μm of positive photoresist was spin-coated onto the samples and baked at 80°C for 2 min [9]. A mask with 1–10 μm wide straight waveguides was used for patterning. Chalcogenide glasses are soluble in soda-containing solutions. For this reason the commercial developer solution used for the positive photoresist can be used to etch the resist and the chalcogenide film in only one process step. In the etching process the samples are fixed on the spin coater. The developer is then poured onto the sample and after approximately 20 s the sample is washed with distilled water and spin-dried. The etch depth is subsequently measured by the profilometer. The photolithography was performed before ion implantation and the channel waveguides thus obtained were used for photoluminescence spectra (PL) and photoluminescence excitation spectra (PLE) measurements. To allow end-fire coupling into the waveguides all samples were cleaved to obtain good quality end-faces.

The waveguides were ion-implanted with 1 MeV Er^+ ions to fluences of 1.0, 3.5, or 7.0×10^{14} ions/cm^2. The 9 nA ion beam was raster-scanned over a 1×1 cm^2 area. No sample cooling was employed. The projected range and range straggling of 1 MeV Er^+ in As_2S_3 are 255 and 76 nm [14]. In one case, a sample received a second ion implantation with 3.5×10^{14} ions/cm^2 of S^+ ions. The energy of 235 keV (at 95 nA) was chosen for best overlap of the erbium and sulphur doping profiles. One series of single- and of multi-layer samples were produced to study the influence of the doping level on the luminescence and lifetime. The main parameters of these samples are summarised in Table 1.

2.2. Characterisation techniques

The chalcogenide composition and the dopant concentration were measured by Rutherford backscattering spectroscopy (RBS) of 4 MeV He^+ ions scattered through 165°. The experimental results were analysed by computer simulations using the rump code [15].

The spectroscopic properties of the samples were characterised by PLE, PL and the measurement of the lifetime τ_2 of the erbium $^4I_{13/2}$ metastable energy level. To measure the PLE spectrum we pumped the waveguides from a tunable, pulsed Ti:sapphire laser (2 ps pulse width at 82 MHz repetition rate). The beam was end-fire coupled by means of a 40× microscope objective. A multimode optical fibre was used to collect the luminescence signal at the end of the waveguide. The collected light was analysed in an optical spectral analyser. To obtain the PLE spectrum we recorded the integral over the luminescence intensity at 1.54 μm as a function of the pump wavelength.

For the PL and lifetime measurements we pumped the samples using a pig-tailed laser diode emitting at 983 nm. In the case of the PL spectra the pump light was coupled into the waveguide directly by a monomode fibre. As in the case of the excitation spectrum the luminescence was collected by a multimode fibre and analysed in an optical spectrum analyser. It is quite difficult to estimate the coupling and waveguide losses for all samples. However, to get a quantitative measurement for the luminescence intensity we normalised the integral over the PL spectrum by the integral over the pump power at the end of the waveguide. This approach is reasonable as the absorption of the pump light by the erbium ions is estimated to be below 0.2 dB, which is small with respect to the insertion losses.

To measure the lifetime τ_2 of the Er^{3+} $^4I_{13/2}$ metastable level, the chopped pump beam (25 Hz) was end-fire coupled into the waveguides by means of a microscope objective (×60 for single-layers, ×40 for multi-layers). The luminescence light at the output face of the sample was focused onto an InGaAs photodetector by means of a microscope objective and a cylindrical lens. The pump light was suppressed by an optical long-pass filter. The decay curve was recorded by a digital oscilloscope and averaged over 25 600 cycles. The oscilloscope was triggered by diffused pump light captured by a second photodiode. This set-up allows the elimination of any influence of the jitter caused by the chopper.

Table 1
Main parameters of studied sample series

	Composition	Er doping (ions/cm^2)	N_{eff} (ions/cm^3)	S doping (ions/cm^2)	Etch depth (μm)
S1	0.4 μm As_2S_3	1.0×10^{14}	1.4×10^{18}	–	0.07
S3		3.5×10^{14}	5.2×10^{18}	–	0.07
S7		7.0×10^{14}	1.0×10^{19}	–	0.05
S3S		3.5×10^{14}	5.2×10^{18}	3.5×10^{14}	0.05
M1	0.5 μm As_2S_3	1.0×10^{14}	4.2×10^{17}	–	–
M3	+0.4 μm $As_{24}S_{38}Se_{38}$	3.5×10^{14}	1.5×10^{18}	–	–
M7	+0.6 μm As_2S_3	7.0×10^{14}	3.0×10^{18}	–	–

3. Results

3.1. Rutherford backscattering

Fig. 1 shows the RBS spectrum of an erbium-implanted As_2S_3 single layer (points) as well as the simulated spectrum (line). Some surface channels are indicated with labeled dotted lines. Going from left to right, the following features can be identified: a ridge at canal 220 which corresponds to the interface between the silicon wafer and the SiO_2 layer, a small peak due to carbon contamination at the surface (likely accumulated during the RBS analysis), a peak due to an $O(\alpha,\alpha)O$ nuclear resonance, a ridge at channel 320 corresponding to oxygen scattering at the interface between the SiO_2 and As_2S_3 layers, a wiggle due to a $Si(\alpha,\alpha)Si$ nuclear resonance (not simulated), and a ridge at channel 500 due to Si scattering at the interface between the SiO_2 and As_2S_3 layers. To the right of the Si edge one can observe: a broad peak due to scattering from sulphur in the As_2S_3 layer, a shoulder due to the 4.2% natural abundance of the ^{34}S isotope, noise due to multiple scattering (not simulated), a large broad peak due to scattering from arsenic in the As_2S_3 layer, and finally a small peak due to the ion implanted erbium, superposed on a background of pile-up events (included in the simulation). The relative height of the S and As peaks shows that the composition is $As_{2.07}S_3X_{0.1}$, close to the nominal composition of As_2S_3. (X being a light element, which cannot be directly detected by RBS. The small amount of X in the As_2S_3 layer has been inferred from the relative As and S peak heights only.) The width of the As and S peaks corresponds to a layer thickness of 1.175×10^{18} at./cm^2, which, combined with the thickness of 400 nm measured by surface profilometry, indicates that the density is only 2.9×10^{22} at./cm^3. From the position and shape of the Er peak relative to the Er surface channel, it is estimated that the Er is distributed roughly Gaussian, centered at 250 nm depth and with a FWHM of 200 nm. The width appears about 10% larger than that due to range straggling only, which can be caused by diffusion or by surface roughness

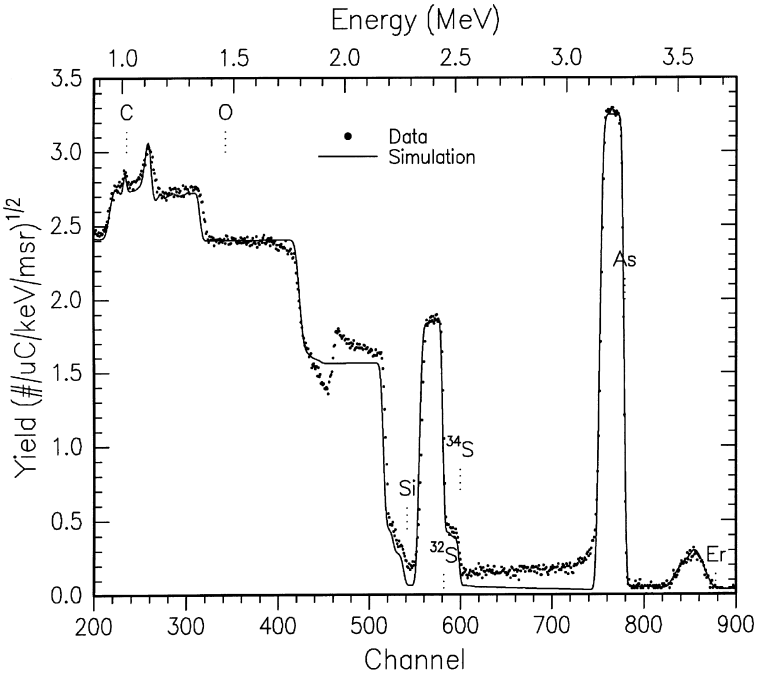

Fig. 1. RBS spectrum of an erbium-implanted As_2S_3 single layer (points) and the simulated spectrum (line).

(sputtering) or both. As well, it is observed that about 5×10^{14} at./cm^2 Er has been implanted into the As_2S_3 layer whereas 3.7×10^{14} at./cm^2 Er ends up in the underlying SiO_2 layer.

Analysis of the multilayer sample (not shown) established the thicknesses and compositions of the three layers: a layer of 1.4×10^{18} at./cm^2 of $As_{26.5}S_{37.7}Se_{35.8}$ is sandwiched between 2.0 and 2.44×10^{18} at./cm^2 thick layers of $As_{1.98}S_3$. The ion-implanted erbium appears again to be distributed roughly Gaussian, with some Er in the middle layer (5.0×10^{14} at./cm^2) and some in the deepest $As_{1.98}S_3$ layer (3.5×10^{14} at./cm^2).

3.2. Thin film geometry

The greatest possible overlap of the guided modes at the pump/signal wavelength and the erbium doping profile is necessary for efficient pump absorption and signal amplification. In Fig. 2, the intensity mode profiles of the fundamental waveguide modes and the erbium doping profile (1 MeV) are shown for the multi-layer samples. The single and multi-layer films are monomode at 1550 nm (signal), but multimode at 980 nm (pump wavelength). We define an effective doping concentration by the product of the overlap integrals of the doping profile with the optical mode profiles at the pump and signal wavelengths

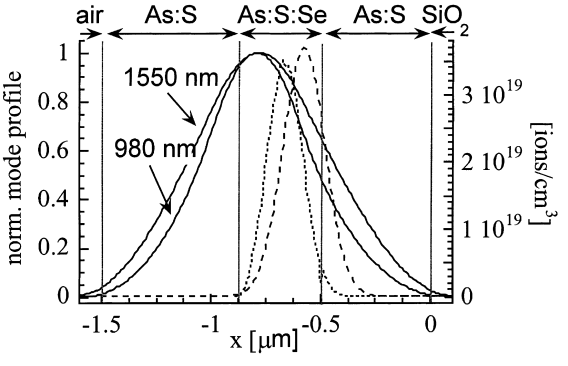

Fig. 2. Intensity profile of the fundamental waveguide modes at 980 and 1500 nm of the multi-layer samples. The nominal/measured erbium doping profiles are represented by the dotted/dashed lines.

$$N_{\text{eff}} = N_0 \frac{\int \tilde{N}(y) I_1(y)\,\mathrm{d}y \int \tilde{N}(y) I_2(y)\,\mathrm{d}y}{\int I_1(y)\,\mathrm{d}y \int I_2(y)\,\mathrm{d}y}. \quad (1)$$

$N(y) = N_0 \tilde{N}(y)$ is the doping profile and $I_{1/2}(y)$ are the intensity profiles of the fundamental waveguide modes at 980 and 1550 nm. For the single-(multi-) layer samples studied in this paper the efficiency is decreased to 0.21 (0.062) of the value of homogeneously doped glass (at the same maximum Er^{3+} concentration). The thin film geometry of the samples has been chosen in order to optimise the overlap for experimentally accessible implantation depths and the waveguide modes. The resulting effective doping concentrations are given in Table 1.

3.3. PLE and PL

Fig. 3 shows the PLE spectrum for a single-layer sample. The result can be reasonably fitted by a Gaussian curve with its maximum at 983 nm and a width of 33 nm. The peak position is identical to the emission wavelength of our pump laser diode.

The emission cross-section spectrum in the 1.54 μm region of the single-layer sample S3 is shown in Fig. 4(a). The maximum of the PL emission is situated at 1536 nm and its width (FWHM) is 45 nm. No significant difference in the shape of the PL spectra was found for all samples investigated. The absolute cross-section values were obtained by scaling the peak cross-section with

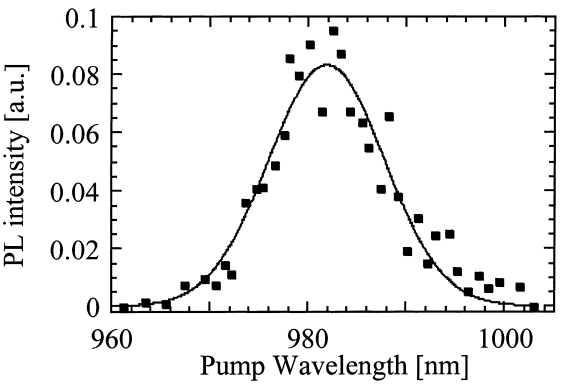

Fig. 3. PLE spectrum of an Er^{3+}-doped As_2S_3 film.

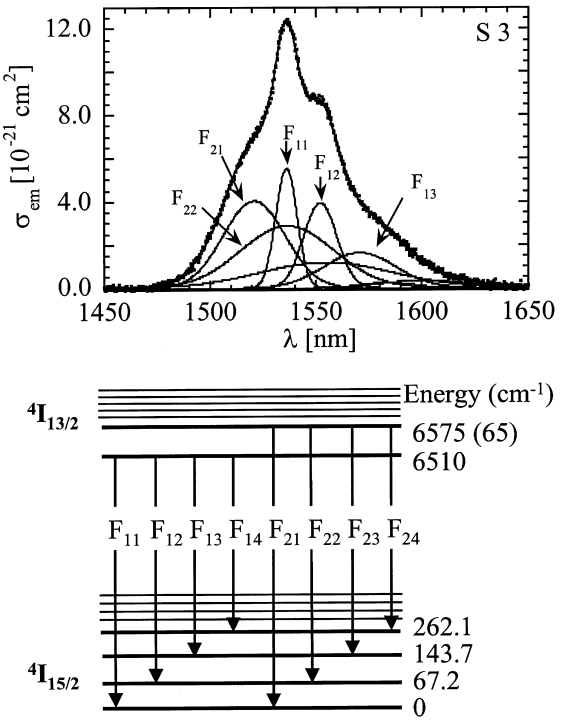

Fig. 4. (a) PL spectrum of Er^{3+}-doped As_2S_3 single-layer. The lines correspond to a calculation based on the Er^{3+} energy diagram shown in (b).

$$\frac{1}{\tau_2} = \frac{8\pi n^2}{c^2} \int v^2 \sigma_{em}\, dv, \tag{2}$$

where τ_2 is the radiative lifetime of the metastable Er^{3+} $^4I_{13/2}$ energy level, n the linear refractive index of the glass host and v is the light frequency. Peak emission cross-sections $\sigma_{em/peak}$ of 1.1 to 1.6×10^{-21} cm^2 were measured (Table 2). The multi-layer samples had slightly higher cross-sections compared to the single-layer ones. Moreover, the post-implantation annealing leads to a small decrease of $\sigma_{em/peak}$.

The normalised luminescence intensity is increasing with the doping level. Significant enhancement of the PL intensity due to sulphur co-implantation was found and the post-implantation annealing leads also to higher PL intensities.

The shape of the PL spectrum can be fitted by a model of the Stark splitting of the $^4I_{13/2}$ and $^4I_{15/2}$ energy levels (Fig. 4(b)). Four (two) energy sublevels were taken into account for the $^4I_{15/2}$ ($^4I_{13/2}$) level. To limit the number of free parameters we assumed that the population of the $^4I_{13/2}$ level is thermalised and that inhomogeneous line broadening (e.g., Gaussian peak shape) is dominant. The experimental data is very well fitted by the theoretical curve. The deduced splitting energies for sample S3 are indicated in Fig. 4(b).

3.4. Lifetime

The lifetime τ_2 of the Er^{3+} metastable energy level was measured to be between 1.6 and 2.3 ms (Table 2). The precision of the lifetime measurement is estimated to ±0.1 ms. No pump intensity dependence of τ_2 or the shape of the decay curves could be found for any sample. The lifetime decreases slightly with increasing erbium concentration. τ_2 is also slightly lower for the multi-layer samples compared to the single-layer samples.

Post-implantation annealing of the single-layer samples increases their lifetimes. But the more interesting feature is the change of the shape of the

Table 2
PL spectral data and lifetimes of studied samples

	As-implanted			Post-implantation-annealed			
	PL int. (% pump)	$\sigma_{em/peak}$ (10^{-21} cm^2)	τ_2 (ms)	PL int. (% pump)	$\sigma_{em/peak}$ (10^{-21} cm^2)	τ_2 (ms)	τ_3 (ms)
S1	0.37	12	2.1	3.6	11	2.3	0.25
S3	2.9	13	2.0	–	–	–	–
S7	7.0	–	–	–	–	–	–
S3S	4.5	13	1.9	27	11	2.3	0.28
M1	–	–	–	1.0	–	–	–
M3	–	–	–	5.6	15	1.6	–
M7	–	–	–	9.2	15	1.7	–

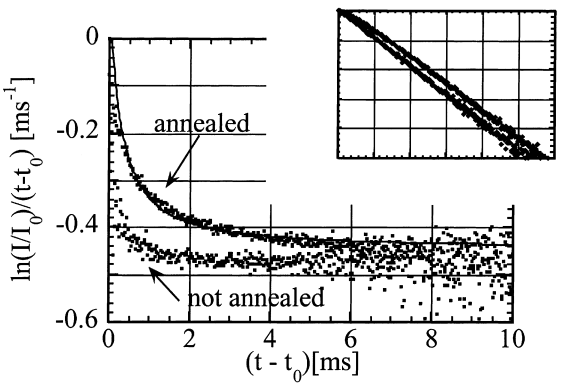

Fig. 5. Plot of the PL decay rate as a function of time for single-layer sample S1 before and after post-implantation annealing. The inset displays the same result in the common logarithmic plot.

decay curves. Fig. 5 displays the decay curve for sample S1 before and after the post-implantation annealing. The inset of the figure shows the normal presentation of lifetime measurements (natural logarithm of PL intensity as a function of time). But to reveal smallest deviations from ideal single-exponential decay we are plotting the normalised PL decay rate defined by $\ln(I/I_0)/(t-t_0)$ as a function of time. In this kind of plot, a pure exponential decay would lead to a horizontal straight line. The steep drop observed at small times (<0.15 ms) results from the finite bandwidth of the detector and has no physical signification. Absolute values of the lifetime τ_2 can be obtained by fitting a horizontal line to the constant section of the decay curve.

The deviation from pure exponential behaviour observed for the annealed sample can be explained by the non-negligible lifetime τ_3 of the Er^{3+} pump level $^4I_{11/2}$. We used a model which neglects direct transitions from the $^4I_{11/2}$ level to the $^4I_{15/2}$ ground state, e.g., the lifetime τ_3 of the pump level depends only on the $^4I_{11/2}$ to $^4I_{13/2}$ transition rate. The experimental data could be fitted by this model using $\tau_3 = 0.25$ ms ($\tau_2 = 2.3$ ms). A similar results was obtained for S3S after annealing ($\tau_3 = 0.28$ ms). This feature was also found for the multi-layer samples. Nevertheless the effect was too small to allow values for τ_3 to be deduced.

4. Discussion

4.1. RBS

The RBS measurements confirm well the film structure and stoichiometry and the erbium doping profile and concentration. However, the measured glass matrix density is quite low. Consequently, the real erbium penetration depth is greater than the nominal ones, which were calculated by using nominal glass density values. This is also the reason for the accidentally high erbium concentration inside the SiO_2 buffer-layer.

4.2. PL intensity

Compared to erbium-doped Al/P-doped silica or fluorophosphate glass fibres [17] the Er^{3+} peak emission cross-sections of As_2S_3 films are about two times higher. This increase of the cross-section is due to the higher linear refractive index of chalcogenide glasses. This is also the reason for the higher cross-sections for the multi-layers in respect with the single-layers. The refractive index of $As_{24}S_{38}Se_{38}$ is $n = 2.43$ which is slightly higher than for As_2S_3 ($n = 2.41$). The PL intensity increases linearly with increasing erbium concentration for single- and multi-layer samples. This result indicates that for the concentrations used there is no interaction between Er^{3+} ions, which could cause parasitic effects such as co-operative up-conversion.

The difference in PL intensity between the single- and multi-layer samples scales with the effective doping rate defined by Eq. (1). This result justifies our model, which, however, neglects the presence of higher order waveguide modes at the pump wavelength. It also shows the great importance of high overlap between the doping profile and the mode profiles.

The crystal field of the glass host splits the Er^{3+} $^4I_{15/2}$ manifold into eight components and the $^4I_{13/2}$ manifold into seven components [17]. It is usually impossible to observe all the resulting transitions and to measure the corresponding Stark splitting energies. The first four (three) splitting energies of the $^4I_{15/2}$ ($^4I_{13/2}$) manifold of an Er^{3+}-doped alumino-silicate glass fiber were

measured by low temperature absorption and emission measurements [18]. The fits to the room temperature PL spectra of our Er^{3+}-doped chalcogenide films allowed the determination of three splitting energies of the ground state and one of the excited states. Compared to the values of Ref. [18], the splitting energies of the doped As_2S_3 films are slightly higher, explaining the wider Er^{3+} PL of our samples.

4.3. Lifetime(s)

The measured lifetime τ_2 of the Er^{3+} $^4I_{13/2}$ metastable energy level is about five times lower than for Er^{3+}-doped silica [18]. This is due to the higher refractive index of chalcogenide glasses, which increases the oscillator strength of the radiative $^4I_{13/2} \rightarrow {}^4I_{15/2}$ transition. On the other hand the non-radiative decay rates are significantly lower due to the low phonon energy of chalcogenide glasses. Hence, the decay rate of the phonon dominated non-radiative $^4I_{11/2} \rightarrow {}^4I_{13/2}$ transition is decreased. In Er^{3+}-doped Ga:La:S glass, lifetimes of the Er^{3+} pump level as high as $\tau_3 = 1.23$ ms were measured [12]. Therefore, the approximation that the lifetime τ_3 is much smaller than the lifetime τ_2 cannot be applied to chalcogenide glasses, and a deviation from a single exponential PL decay can be observed in the lifetime measurements. This effect was found to be strong enough to deduce values of τ_3 from standard lifetime measurements.

4.4. Post-implantation annealing

The post-implantation annealing enhances significantly the PL intensity. But the emission cross-section is only slightly affected by the annealing. The increase of the PL intensity is hence attributed to the activation of erbium ions. The Er^+ ions entering the glass target do not necessarily stop in active sites inside the glass matrix. The atomic rearrangement during the post-implantation annealing allows more erbium ions to find active sites and the overall PL intensity is increased. Similar results were already reported for soda-lime silica glass [13].

Significant pump level lifetimes were observed only for post-implantation annealed samples. Annealing at temperatures near the glass transition temperature of the matrix allows the curing of defects introduced by the ion implantation. For the as-implanted samples these defects act as local phonon sources which couple to the Er^{3+} ions. As a result the Er^{3+} pump level is rapidly depopulated and τ_3 is no longer measurable in our experiment. The slightly lower values of τ_2 for as-implanted samples can be explained by the same reasoning.

4.5. Sulphur co-implantation

We found that sulphur co-implantation of the erbium-doped chalcogenide films increases significantly the Er^{3+} PL intensity at 1.54 μm. The prospected aim of this co-doping was to increase the sulphur coordination of the already implanted erbium ions. This work was motivated by results on erbium-doped silica glass. It has been shown that erbium is coordinated in silica with about 6 oxygen atoms in a first shell and that there are no direct Er–Si bonds [16]. Furthermore, these ErO_6 complexes can be related to the active sites of the Er^{3+} ions. In analogy to this result we suppose that an increase of the sulphur coordination of the erbium ions should increase the transition rate of erbium to its active Er^{3+} state. The higher PL intensity of the sulphur co-doped sample (S3S) justifies this approach.

5. Conclusion

As_2S_3 single-layers and $As_2S_3/As_{24}S_{38}Se_{38}/As_2S_3$ multi-layers were fabricated by thermal evaporation. Ion implantation was used for erbium doping of these samples. Channel waveguides were fabricated using a wet-etching technique. High emission cross-sections at 1.54 μm and small radiative lifetimes of the Er^{3+} metastable energy level were measured. Significant lifetimes of the Er^{3+} $^4I_{11/2}$ pump level were observed. The active properties could be enhanced by post-implantation annealing or sulphur co-implantation. These results demonstrate the dramatic difference between chalcogenide and silica glass.

In this paper, we report first results. There is still a great potential for further enhancement of the active properties of the samples by optimising the fabrication and doping procedures. However, taking into account the already noted spectral properties, erbium-doped chalcogenide glass films will offer advantages over silica glass in integrated optics applications.

Acknowledgements

We acknowledge financial support from a National Science Engineering Research Council strategic grant sponsored by Exfo Ingénérie and Lucent Technologies. J.F. acknowledge CNRS for the possibility to stay at COPL and NATO for financial support. K. Le Foulgoc is greatly acknowledged for her invaluable help in the sample fabrication.

References

[1] T.V. Galstian, J.F. Viens, A. Villeneuve, K.A. Richardson, M.A. Duguay, J. Lightwave Technol. 15 (1997) 1343.
[2] K.A. Cerqua-Richardson, J.M. McKinley, B. Lawrence, S. Joshi, A. Villeneuve, Opt. Mater. 10 (1998) 155.
[3] S. Ramachandran, S.G. Bishop, Appl. Phys. Lett. 73 (1998) 3196.
[4] K.E. Youden, T. Grevatt, R.W. Eason, H.N. Rett, R.S. Deol, G. Wylangowski, Appl. Phys. Lett. 63 (1993) 12.
[5] T. Katsuiyana, S. Satoh, H. Matsumura, Appl. Phys. Lett. 59 (1986) 5.
[6] C. Meneghini, J.F. Viens, A. Villeneuve, É.J. Knystautas, M.A. Duguay, K.A. Richardson, JOSA B 15 (1998) 1305.
[7] I.Z. Indutnyi, P.E. Shepeljavi, J. Non-Cryst. Solids 227–230 (1998) 700.
[8] O. Nordman, N. Nordman, N. Peyghambarian, J. Appl. Phys. 84 (1998) 6055.
[9] J.F. Viens, C. Meneghini, A. Villeneuve, T. Galstian, É.J. Knystauktas, M.A. Duguay, K.A. Richardson, T. Cardinal, J. Lightwave. Technol. 17 (1999) 1184.
[10] S.Q. Gu, S. Ramachandran, E.E. Reuter, D.A. Turnbull, J.T. Verdeyen, S.G. Bishop, J. Appl. Phys. 77 (1995) 3365.
[11] A.S. Oliveira, M.T. de Araujo, A.S. Gouveia-Neto, J.A. Medeiros Neto, A.S.B. Sombra, Y. Messaddeq, Appl. Phys. Lett. 72 (1998) 753.
[12] C.C. Ye, D.W. Hewak, M. Hempstead, B.N. Samson, D.N. Payne, J. non–Cryst. Solids 208 (1996) 56.
[13] A. Polman, Appl. Phys. Rev. 82 (1997) 1, references therein.
[14] J.F. Ziegler, J.P. Biersack, U. Littmark, The Stopping and Range of Ions in Solids, Pergamon, New York, 1995.
[15] L.R. Doolittle, Nucl. Instrum. and Meth. B 15 (1986) 227; http://www.genplot.com.
[16] M.A. Marcuse, A. Polman, J. non–Cryst. Solids 136 (1991) 260.
[17] W.J. Miniscalco, R.S. Quimby, Opt. Lett. 16 (1991) 258.
[18] E. Desurvire, J.R. Simpson, Opt. Lett. 15 (1990) 547.